Applied Catalysis B: Environmental 138–139 (2013) 113–121

Contents lists available at SciVerse ScienceDirect

Applied Catalysis B: Environmental

journal homepage: www.elsevier.com/locate/apcatb

# ZrNO–Ag co-sputtered surfaces leading to *E. coli* inactivation under actinic light: Evidence for the oligodynamic effect

S. Rtimi[a,b,*], M. Pascu[c], R. Sanjines[d], C. Pulgarin[a,**], M. Ben-Simon[e], A. Houas[a], J.-C. Lavanchy[f], J. Kiwi[g]

[a] UR Catalyse et Matériaux pour l'Environnement et les Procédés (URCMEP), Faculté des Sciences de Gabès, Université de Gabès, 6072,Gabès, Tunisia
[b] Ecole Polytechnique Fédérale de Lausanne, EPFL-SB-ISIC-GPAO, Station 6, CH-1015 –,Lausanne, Switzerland
[c] Ecole Polytechnique Fédérale de Lausanne EPFL-BCH-LCS, 1015 Lausanne, Switzerland
[d] Ecole Polytechnique Fédérale de Lausanne, EPFL-SB-IPMC-LNNME, Bat PH, Station 3, CH-1015 Lausanne, Switzerland
[e] Ecole Polytechnique Fédérale de Lausanne, EPFL-ENAC-IIEGR-CEL, Bat GC, Station 18, CH-1015 Lausanne, Switzerland
[f] Université de Lausanne, IMG, Centre d'Analyse Minérale, Bat Anthropole, CH-1015 Lausanne, Switzerland
[g] Ecole Polytechnique Fédérale de Lausanne, EPFL-SB-ISIC-LPI, Bat Chimie, Station 6, CH-1015 Lausanne, Switzerland

ARTICLE INFO

*Article history:*
Received 12 October 2012
Received in revised form 21 January 2013
Accepted 28 January 2013
Available online 21 February 2013

*Keywords:*
ZrNO sputtering
ZrNO–Ag co-sputtering
*E. coli*
Oligodynamic effect

ABSTRACT

This study reports visible light sensitive ZrNO and ZrNO–Ag polyester samples prepared by sputtering in an $Ar/N_2/O_2$ atmosphere leading to *Escherichia coli* bacterial inactivation. The bacterial inactivation by ZrNO avoids the increasing environmental concern involving the fate of Ag-leaching of many disinfectants. The simultaneous co-sputtering of ZrNO and $Ag_2O$ enhanced the *E. coli* bacterial inactivation kinetics compared to the sequential sputtering of ZrNO and Ag. A reaction mechanism is suggested triggered by photoinduced interfacial charge transfer (IFCT) suggesting electron injection form the $Ag_2O_{cb}$ to the $ZrO_{2cb}$. The sizes of the $ZrO_2$ and Ag nanoparticles in the co-sputtered ZrNO–Ag were 80–130 nm and 8–15 nm respectively as determined by high angular annular dark field (HAADF) microscopy. Evidence is presented by X-ray photoelectron spectroscopy (XPS) for the self-cleaning of the photocatalysts after bacterial inactivation. This enabled a stable catalyst reuse. The XPS experimental spectra of ZrNO and ZrNO–Ag were deconvoluted into their ZrN, ZrNO and $ZrO_2$ components. The amounts of Ag-ions released during bacterial inactivation were < 5 ppb/cm$^2$ and well below the Ag cytotoxic levels. Since no cytotoxicity was introduced during the bacterial inactivation process, the ZrNO–Ag disinfection proceeds through an oligodynamic effect.



## 1. Introduction

Antimicrobial nanoparticulate films preparation is a topic of increasing attention since their objective is to reduce or eliminate the formation of infectious bacteria biofilms leading to hospital acquired infections (HAI) [1–4]. But more effective bacterial inactivation are needed due to the increasing resistance of pathogenic bacteria to synthetic antibiotics administered for long times [5]. Also nosocomial infections due to antibiotic resistant bacteria are becoming more frequent developing into a serious problem associated with high health care costs. Recently, Mills et al. [6], Parkin et al. [7–10], Foster et al. [11], Dunlop et al. [12] and Yates et al. [13] have reported antibacterial Ag, Cu, and $TiO_2$ coatings on glass and polymer films depositing the metal/oxides by CVD and sputtering techniques. Our laboratory has reported the antibacterial properties and kinetics of Ag- and Cu-modified textiles deposited by DC-magnetron, pulsed DC-magnetron and high power impulse magnetron sputtering (HIPIMS). Kelly has reported TiN and other nitrides co-sputtered with Ag able to inactivate Gram-negative and Gram-positive bacteria in the dark [14,15].

The benefits of the ZrNO films obtained by DC-sputtering in a reactive environment (in the presence of $O_2$) compared the colloidal prepared films is in the microstructure of the films showing: uniformity, ability to control of the film thickness, improved adhesion and frequently fast bacterial inactivation kinetics. Colloidal deposited $TiO_2$ films are non-uniform, not mechanically stable present low adhesion and can be wiped off by using a cloth or a thumb [16].

Another benefit found when using ZrNO and ZrNO–Ag films is due to the nitride absorption in the visible range. This avoids doping like in the $TiO_2$ to extend the $TiO_2$ absorption into the visible region.

* Corresponding author at: Ecole Polytechnique Fédérale de Lausanne, EPFL-SB-ISIC-GPAO, Station 6, CH-1015 Lausanne, Switzerland. Tel.: +41 216936150.
** Corresponding author at: Ecole Polytechnique Fédérale de Lausanne, EPFL-SB-ISIC-GPAO, Station 6, CH-1015 Lausanne, Switzerland. Tel.: +41 216934720.
*E-mail address:* sami.rtimi@epfl.ch (S. Rtimi).

0926-3373/$ – see front matter © 2013 Elsevier B.V. All rights reserved.
http://dx.doi.org/10.1016/j.apcatb.2013.01.066

Doping decreases considerably the photo-activity of the films compared to pristine $TiO_2$ [17–19].

In the last section of the present study, the mechanism of the bacterial inactivation mediated by ZrNO–Ag is discussed. Recently, we have reported the mechanism of the damage induced by $TiO_2$ photocatalysis on the bilayer cell-envelope of *Escherichia coli* in several studies [20–23]. Other groups working in the disinfection field have also addressed the mechanism of disinfection [24–27]. The *E. coli* and MRSA viability as a function of time was monitored by direct transfer on plate and by stereomicroscopy. These two methods were used to determine the bacterial viability because they imply a very low experimental bias [28,29]. No bacterial regrowth was observed after bacterial inactivation. showing that the bacterial cells were not more viable.

The electronic properties of transition-metal oxy-nitrides (MeO*x*N*y*) in general and the optical properties like zirconium oxynitrides (ZrO*x*N*y*) in particular have recently attracted considerable interest. These materials are used as gate dielectrics [30] temperature sensors in magnetic fields [31], corrosion resistance coatings [32] and decorative films (golden, gray and black tones) [33,34]. But these oxynitrides have been poorly explored for the inactivation of micro-organisms/bacteria. $ZrO_2$ is a material with a band-gap of 5.0 eV and a flat band potential of −1.0 eV *vs* NHE more negative than the potential $H_2/H_2O$. Its valence hole potential is more positive than 1.23 eV NHE, pH 0 required for $O_2/H_2O$. The band-gap for $ZrO_2$ nanoparticles is 3.2 and 3.0 eV [35]. Defects in their structure have been reported to play a role in $ZrO_2$ donor to acceptor electron transfer reactions [36].

Our laboratory has recently published studies involving nitrides and oxy-nitrides [37]. Catalytic and photocatalytic disinfection of bacteria was reported using nitride sputtered samples. Reactive sputtering in the presence of $O_2$ introduces ionic metal–oxygen species in an N-matrix. $ZrO_2$ is a photosensitive oxide and the trapping of the carriers induced by light has been shown to be important during bacterial inactivation.

Antimicrobial Ag-nanoparticles (NPs) have sputtered [9,18,28,29] on different textiles due to the known disinfecting properties of Ag. Ag is also used in healing wound-pads [4–6], and implants [1]. The Ag-ions on responsible for the bacterial disinfection diffuse through the bacteria cell wall porins into the cell interior, leading to bacterial disinfection without inducing cytotoxicity. The bactericidal mechanism of Ag-ions implying: (i) condensation of DNA affecting bacterial replication, and (ii) interaction with protein-thiol groups leading to protein damage.

Magnetron sputtering has been used to deposit thin metal/oxide films (or combinations thereof) inducing self-cleaning and antibacterial properties in natural fibers like cotton and artificial textiles like polyester [14,15,28,29,37]. The present study addresses: (a) the sputtering of ZrNO and ZrNO–Ag films on polyester optimizing the sputtering chamber gas atmosphere to attain the fastest *E. coli* bacterial inactivation kinetics, (b) the performance of ZrNO–Ag films obtained either by sputtering sequentially Ag after Zr or by co-sputtering of both components, (c) the bacterial inactivation kinetics by ZrNO and ZrNO–Ag films under low intensity actinic light and finally (d) the characterization of the microstructure of ZrNO and ZrNO–Ag films by X-ray fluorescence (XRF), diffuse reflectance spectroscopy (DRS), atomic force microscopy (AFM), contact angle (CA) and transmission electron microscopy (TEM).

## 2. Experimental

### 2.1. DC and DCP sputtering procedures

DC-magnetron sputtering of metals/oxides and semiconductor particulate has been carried out on textiles in our laboratory [37]. In the sputtering chamber the pressure was set at 0.1 Pa and the substrate-to-target distance was 10 cm. Before the deposition of the films the residual pressure Pr in the sputtering chamber was $Pr \leq 10^{-4}$ Pa. The two inches diameter or 5 cm Zr-cathode was obtained from Lesker Corp, Hastings, East Sussex, UK. During the deposition of ZrNO on the polyester, we determined the most appropriate gas composition being: 5% $N_2$:5% $O_2$:90% Ar. We varied the % gas flow of $N_2$ and $O_2$ maintaining at a fix value the flow of Ar. The gas composition of 5% $N_2$:5% $O_2$:90% Ar allowed to prepare the ZrNO–Ag coatings sputtering for 90 s leading to the shortest time to attain total loss of bacterial viability (40 min, as shown in Fig. 1c).

Oxygen is more reactive than nitrogen. Due to the higher $O_2$ reactivity, the addition of $O_2$ to a sputtered nitride film induces a different microstructure for the metal-bonds in the matrix of the covalent metal–nitrogen bond [14,15]. The effect of $O_2$ concentration is reflected in the color of the nitride samples sputtered during this study. The Zr DC-sputtering was carried out at 280 mA and a bias voltage of −330 V (90 W). The polyester samples were 2 cm × 2 cm in size. Four polyester squares 2 cm × 2 cm were mounted in a round support, receiving the incoming sputtered particles in an homogeneous way as verified in many systems in our laboratory.

Direct current pulsed magnetron sputtering (DCP) was used to sputter Ag on ZrNO at 50 kHz with a 15% reversed voltage. The DCP-sputtering consisted of continuous pulses of 10 μs (280 mA, 198 W). The bias voltage was −500 V during ZrNO deposition and then switched to +75 V during Ag deposition (15% of −500 V). The co-sputtering of Zr and Ag was carried out in a way was similar to the one recently reported [37].

The polyester was a Eidgenössiche Material und Prüfungs Anstalt (EMPA) test cloth sample No. 407, 130 μm thick. It is a polyester Dacron polyethylene-terephthalate; type 54 spun, plain weave ISO 105-F04 used for color fastness determinations. The thermal stability of Dacron polyethylene terephthalate was 115 °C for long-range operation and 140 °C for times ≤1 min.

The calibration of films thickness by the DC-sputtering of the ZrNO layers and DCP-sputtering of Ag on Si-wafers were determined with a profilometer (Alphastep500, TENCOR) and the experimental values were in error of ±10%.

### 2.2. X-ray fluorescence determination of Ag and Zr content on polyester

The Ag- and Zr-content of the polyester was evaluated by X-ray fluorescence in a PANalytical PW2400 spectrometer.

### 2.3. Evaluation of the loss of bacterial

The samples of *Escherichia coli* (*E. coli* K12) was obtained from the Deutsche Sammlung von Mikro-organismen und Zellkulturen GmbH (DSMZ) ATCC23716, Braunschweig, Germany to test the loss of bacterial viability on the Ag-polyester as previously reported by our laboratory [21,28,37]. The bacterial data reported were replicated three times. To verify that no re-growth of *E. coli* occurs after the first inactivation cycle, the ZrNO–Ag samples were incubated for 24 h at 37 °C. Then the bacterial suspension of 100 μL was deposited on three Petri dishes to obtain the replica samples for the bacterial counting. The bacterial counting data reported were replicated three times. No bacterial re-growth was observed.

The statistical analysis of the results was performed for the decrease of the bacterial CFU values reporting the standard deviation values for the runs showing the fastest bacterial inactivation.

The removal of the inoculated bacteria was tested by incubation of the sample on a Petri dish. After 24 h at 37 °C, very few colonies (1–7 colonies) or 99.9% of the inoculated bacteria were extracted and transferred from the polyester fabric into the saline solution.

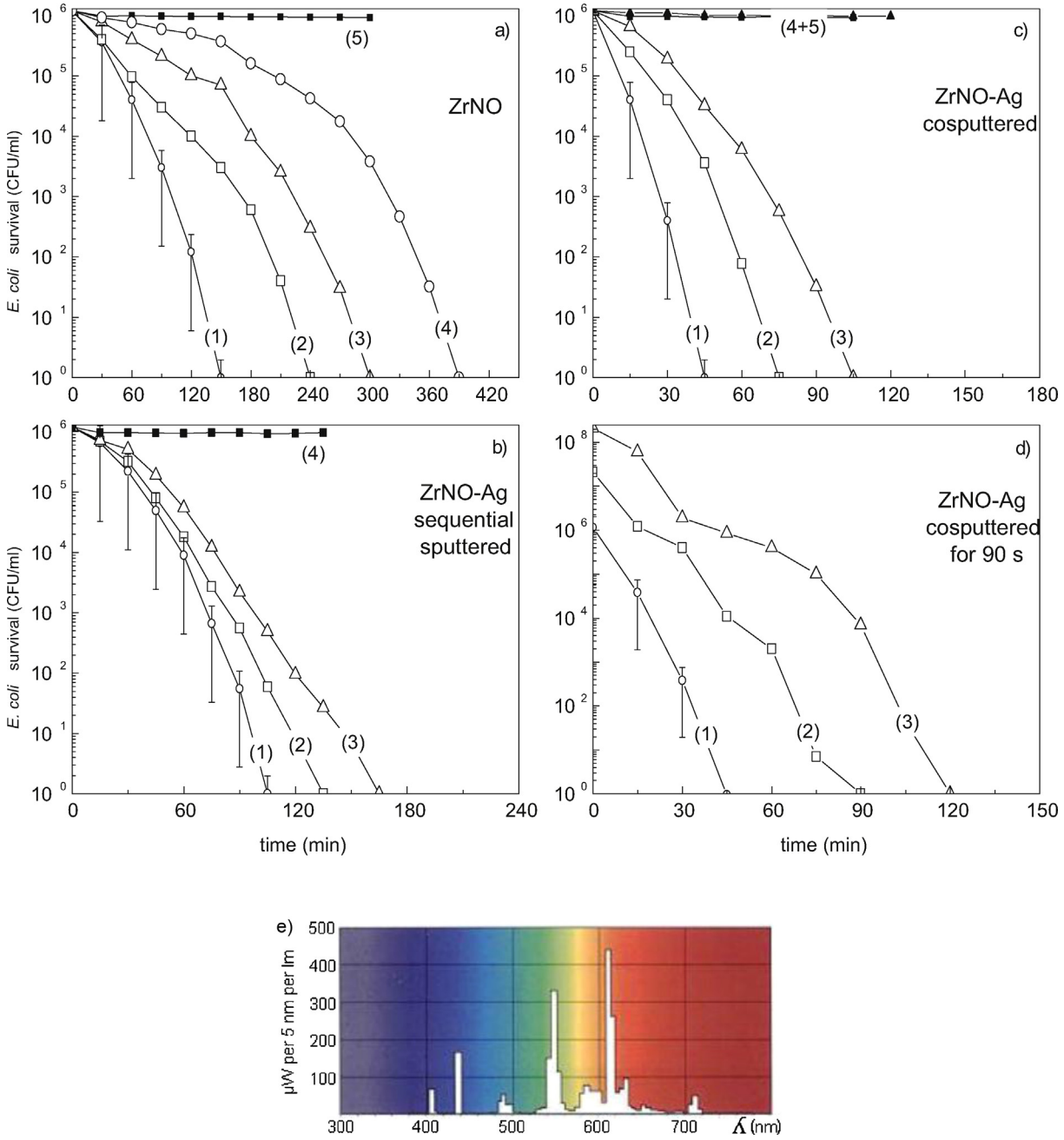


**Fig. 1.** (a) *E. coli* loss of viability by ZrNO as a function of time for: (1) Zr sputtered for 90 s on polyester; (2) Zr sputtered for 150 s; (3) Zr sputtered for 60 s; (4) Zr sputtered for 40 s, The samples were irradiated with an Osram Lumilux 18/827 actinic lamp and finally (5) Zr sputtered for 90 s on polyester but in dark runs. (b) Zr sputtered on polyester for 90 s, followed by Ag-deposition for: (1) Ag 10 s; (2) Ag 20 s; (3) Ag 40 s, under Osram Lumilux 18/827 actinic lamp irradiation and finally (4) Zr sputtered on polyester for 90 s showing the loss of viability. (c) ZrNO–Ag co-sputtered on polyester (1) for 90 s; (2) for 60 s and (3) for 150 s. Runs under illumination under an Osram Lumilux 18/827 actinic light, (4) Zr sputtered on polyester for 90 s in the dark and (5) polyester alone. (d) Effect of the initial concentration on the loss of viability of *E. coli* on a cosputtered ZrNO–Ag (90 s) sample under an Osram Lumilux 18/827 light. (e) Emission spectrum of the Osram Lumilux 18 W/827 lamp.

### *2.4. Diffuse reflectance spectroscopy of polyester samples*

Diffuse reflectance spectroscopy was carried out using a Perkin Elmer Lambda 900 UV-VIS-NIR spectrometer provided for with a PELA-1000 accessory within the wavelength range of 200–800 nm having a resolution of 1.0 nm. The absorption spectra of the samples were plotted in Kubelka–Munk (KM) arbitrary unit *vs* wavelength.

### *2.5. Light irradiation source*

The irradiation of polyester samples was carried out in a closed cavity by Osram Lumilux 18 W/827 actinic lamps emitting between 400 and 700 nm. Each lamp had an integral output of 1.2 mW/cm$^2$ resembling the light distribution in the solar irradiation. These actinic lamps are used generally in hospitals emitting light in the visible region and provide an efficient compromise of energy consumption per unit of luminous flux.

### *2.6. Inductively coupled plasma sector field mass spectrometry (ICPS-MS)*

The FinniganTM ICPS used was equipped with a double focusing reverse geometry mass spectrometer with an extremely low background signal and a high ion-transmission coefficient. The spectral

signal resolution was $1.2 \times 10^5$ cps/ppb and a detection limit of 0.2 ng/L.

### 2.7. X-ray photoelectron spectroscopy (XPS) of the sputtered samples

An AXIS NOVA photoelectron spectrometer (Kratos Analytical, Manchester, UK) equipped with monochromatic Al Kα ($h\nu$ = 1486.6 eV) anode was used during the study. The electrostatic charge effects on the samples were compensated by means of the low-energy electron source working in combination with a magnetic immersion lens. The quantitative surface atomic concentration of some elements was determined from peak areas using sensitivity factors and spectrum corrections [42]. The XPS spectra for the Ag- and Zr-species were analyzed by means of spectra deconvolution software (CasaXPS-Vision 2, Kratos Analytical, UK).

### 2.8. Transmission electron microscopy (TEM) of ZrNO–Ag samples

A Philips CM-12 (field emission gun, 300 kV, 0.17 nm resolution) microscope at 120 kV was used to measure grain size of the Ag-films. The textiles were embedded in epoxy resin 45359 Fluka and the fabrics were cross-sectioned with an ultramicrotome (Ultracut E) at a knife cutting angle of 35°. The energy-diffuse X-ray spectroscopy (EDX) images of the ZrNO–Ag samples were obtained by high angular annular dark field imaging (HAADF).

## 3. Results and discussion

### 3.1. Thickness of Ag, ZrNO and ZrNO–Ag films on polyester

DCP sputtering Ag-ions on polyester led within 1 s to a thickness of 1.2 nm ± 10% equivalent to ~5 layers 0.2 nm thick. The rate of deposition of Ag is $5 \times 10^{15}$ atoms/cm$^2$ s if taking in the lattice the distance of 0.3 nm between Ag-atoms [29]. A film obtained by sputtering is always less dense than the bulk material, so probably the indicated thickness is lower than the real thickness.

A ZrNO-coating thickness of 120 nm was sputtered within 90 s at 280 mA. The co-sputtered Zr–Ag layers leads to a 180 nm thickness within 90 s. This film is thinner than the film obtained by sputtering sequentially Ag on ZrNO on polyester indicating the formation of hybrid composite Zr–Ag layers.

### 3.2. Bacterial inactivation on ZrNO and ZrNO–Ag-polyester

Fig. 1a shows that ZrNO-sputtered polyester samples under low intensity actinic light (4 mW/cm$^2$) within 150 min a bacterial reduction from $10^6$ CFU/ml to undetected bacteria. Fig. 1a, trace 1 includes the statistical analysis of the data for the sample leading to the fastest inactivation as described in Section 2. No re-growth was observed after the first inactivation cycle for ZrNO and ZrNO–Ag materials using the CFU monitoring methods described in Section 2.

Fig. 1b shows that the bacterial inactivation of *E. coli* by ZrNO–Ag samples under low intensity actinic light. Within ~115 min a bacterial reduction from $10^6$ CFU/ml to undetected bacteria was observed. Only marginal improvement was observed in the bacterial inactivation kinetics in Fig. 1b compared to Fig. 1a.

Fig. 1c shows that ZrNO–Ag co-sputtered for 90 s on polyester leads to a 6 $\log_{10}$ bacterial reduction within 45 min. The co-sputtered ZrNO–Ag for 90 s lead to the loss of viability within 40–45 min in Fig. 1c, trace 1. This time to obtain the total loss of viability is much shorter compare to the time to the sequentially sputtered ZrNO (90 s)–Ag (10 s) sample reporter in Fig. 1b. Therefore, co-sputtering Zr–Ag is shown to lead to a faster loss in the bacterial viability as seen in Fig. 1c.

The polyester fabrics were sterilized by autoclaving at 121 °C for 2 h. The 20 μL culture aliquots with an initial concentration of about $10^6$ CFU mL$^{-1}$ in NaCl/KCl (pH 7) were placed on coated and uncoated (control) polyester fabric. The samples were placed on Petri dishes provided with a lid to prevent evaporation. After each determination, the fabric was transferred into a sterile 2 mL Eppendorf tube containing 1 mL autoclaved NaCl/KCl saline solution. This solution was subsequently mixed thoroughly using a Vortex for 3 min. Serial dilutions were made in NaCl/KCl solution. A 100-μL sample of each dilution was pipetted onto a nutrient agar plate and spread over the plate using standard plate method.

The polyester is a micro-porous substrate and distributes the inoculum evenly on the ZrNO, ZrNO–Ag films without needing an adsorption stage. A well-dispersed non-heterogeneous contact is established between the sample and the bacterial solution. In Section 3.9 we suggest the mechanism for the photo-activated ZrNO, ZrNO–Ag trigger interfacial charge transfer leading to the formation of reactive oxidative species leading to the bacterial loss of viability.

### 3.3. X-ray fluorescence of ZrNO and ZrNO–Ag sputtered samples

The Ag- and Zr-contents of the samples were determined by X-ray fluorescence. The weight percentage of Ag for sputtering times of 10 s, 20 s and 30 s, was 0.06, 0.13 and 0.14 wt%/wt polyester, respectively. The weight percentage of Zr for sputtering times of 10 s, 20 s and 30 s, was 0.096, 0.108 and 0.195 wt%/wt polyester, respectively. The co-sputtered ZrNO–Ag (90 s) sample had a Zr-content of 0.06-wt% Zr/wt polyester besides an Ag-0.1 wt% Ag/wt polyester.

Samples with a higher Ag-loading allowed longer bacterial survival times. Fig. 1b shows that for sequential Ag sputtered samples, the inactivation time becomes slower when sputtering for 20 and 40 s Ag on the base layer of ZrNO sputtered for 90 s. The reason for the longer inactivation kinetics is that longer Ag sputtering times leads to a thicker coating of Ag on the ZrNO photoactive layers. This

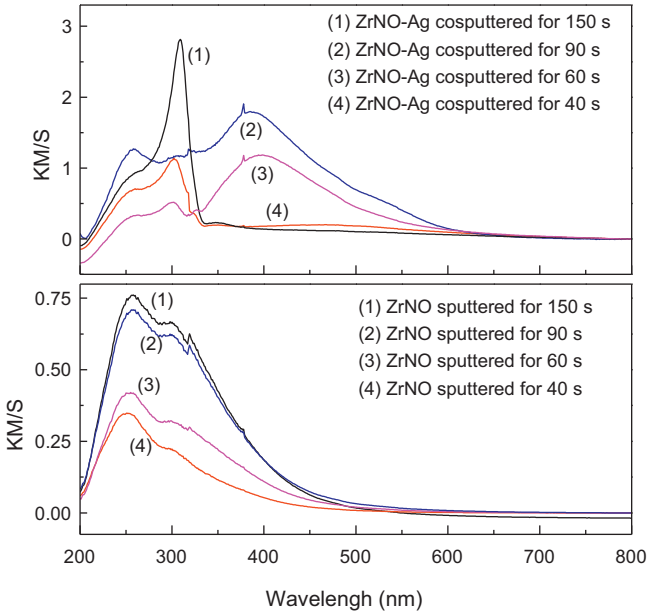


**Fig. 2.** Diffuse reflectance spectra for ZrNO and ZrNO–Ag sputtered on polyester for times as indicated in the figure legends.

hinders the ZrNO photocatalytic contribution leading to the loss of *E. coli* viability.

Fig. 1c shows the faster inactivation kinetics for a 90 s co-sputtered sample in trace 1. Sputtering for only 60 s did not deposit enough catalyst layers to absorb the incident actinic light as shown in trace 2. A longer bacterial inactivation within 105 min (trace 3) was observed for co-sputtered samples for 150 s. These samples showed a longer inactivation time due to the formation of darker Ag-aggregates with a bigger size hindering the light absorption by ZrNO.

### 3.4. Survival kinetics as a function of the initial concentration and light dose

Fig. 1d shows the bacterial inactivation kinetics of *E. coli* on the co-sputtered ZrNO–Ag (90 s) sample with an initial CFU concentrations of: $10^8$, $5 \times 10^7$ and $10^6$. It is readily seen that the inactivation of higher bacterial concentrations need longer time. This observation makes it possible to exclude a strong absorption of *E. coli* K12 on the co-sputtered ZrNO–Ag (90 s) sample. Adsorption of *E. coli* on the 30 nm particles is not possible since the size of the ellipsoidal shape *E. coli* K12 is ~1 μm [118]. The bacterial inactivation kinetics mediated by co-sputtered ZrNO–Ag (90 s) samples, were carried out applying three different light doses from the Lumilux Osram 18 W/827 lamp. This indicated that the bacterial inactivation kinetics was strongly dependent on the applied light dose in the reactor cavity.

### 3.5. Diffuse reflectance spectroscopy (DRS)

Fig. 2 presents the sample DRS spectra in Kubelka–Munk units. The UV–vis reflectance rough data cannot be used directly to assess the absorption of the loaded polyester because of the large scattering contribution of polyester to the reflectance spectra. Normally it is assumed a weak dependence of the scattering (S) on the wavelength when taking DRS spectra. The KM/S values in Fig. 2 allow the

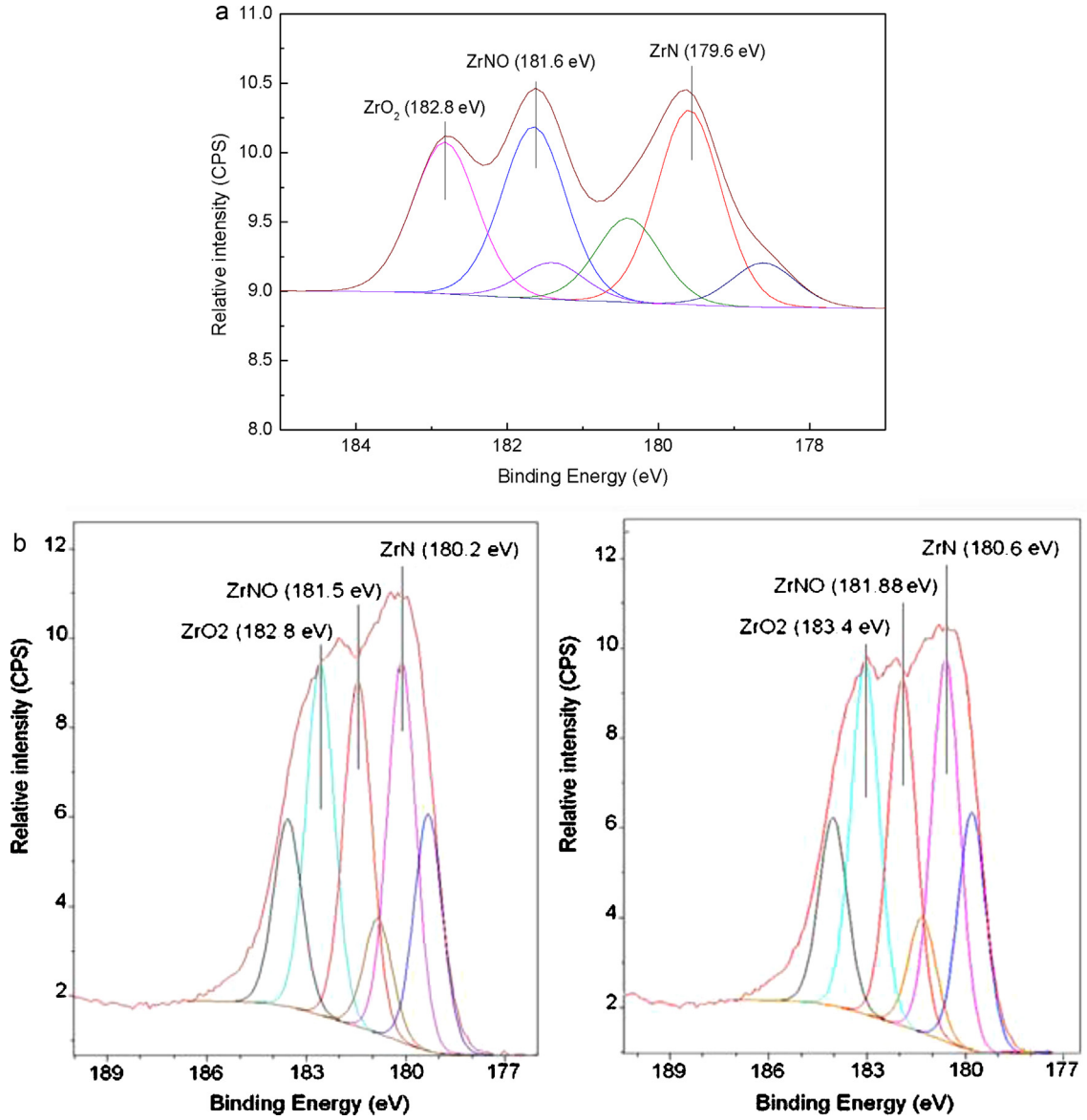


**Fig. 3.** (a) XPS deconvoluted doublets of a ZrNO sputtered sample for 90 s sample contacted for 3 s with bacteria (for other details see text). (b) XPS (left side) deconvoluted doublets of a co-sputtered ZrNO–Ag (90 s) sample contacted for 3 s with bacteria at time zero. Right-hand side: XPS of the deconvoluted doublets after total loss of bacterial viability within 45 min.

**Table 1**
Surface atomic percentage concentration of elements of co-sputtered ZrNO–Ag (90 s).

| | O1s | N1s | C1s | Zr3d | Ag3d |
|---|---|---|---|---|---|
| ZrNO/Ag (90 s) | 14.24 | 4.22 | 23.99 | 10.79 | 39.67 |

correlation of the spectral intensity of the ZrNO–Ag co-sputtered and of the ZrNO samples spectra with the bacterial inactivation kinetics shown in Fig. 1. The Increase in reflectance in the co-sputtered spectra compared to the sequentially sputtered layers in Fig. 2 is due to the different microstructure of the ZrNO–Ag photocatalyst in both cases as shown by TEM in Fig. 7.

The red shifted absorption in the nanoparticles of ZrNO–Ag show the appearance of a red tail in the DRS spectra of the nanoparticles in Fig. 2. Fig. 2 shows around 400 nm the localized surface resonance of the Ag-plasmons. Gunawan et al. [38] recently reported that the oxidation of silver from $Ag^0$ to $Ag_2O$ is a reversible reaction increasing the surface plasmon resonance.

### 3.6. XPS analysis of sputtered samples

Fig. 3a shows the deconvoluted ZrNO sample sputtered 90 s on polyester and contacted for 3 s with bacteria. The experimental envelope was deconvoluted in three doublets by the CasaXPS Vision 2 software and the peaks assigned according to Wiame et al. [39] and Rizzo et al. [40] for: (a) ZrN at 179.6.2 eV, (b) ZrNO at 181.6 eV and (c) $ZrO_2$ at 182.8 eV. The percentage areas of the deconvoluted peaks in the ZrNO experimental XPS envelope were: ZrN 35.37%, ZrNO 33.76% and $ZrO_2$ 30.87%.

Fig. 3b shows the XPS envelope of the ZrNO–Ag co-sputtered (90 s) sample contacted 3 s with bacteria after 45 min leading to the total loss of viability. The deconvoluted peaks were found at: (a) ZrN, 180.2 eV, (b) ZrNO, 181.6 eV and (c) $ZrO_2$, 182.8 eV. The percentage area in Fig. 3b were: ZrN 32.13%, ZrNO 33.90% and $ZrO_2$ 33.97% and were similar for ZrNO and ZrNO–Ag samples. The *y*-axis shows that the counts intensity in the relative scale varies between 8 and 11 for the ZrNO samples and zero to 12 for the ZrNnO–Ag samples. This reflects a stronger charge transfer in the ZrNO–Ag samples due to the Ag presence. We have determined the surface atomic percentage concentration of elements of ZrNO–Ag co-sputtered (90 s) is shown in Table 1.

From Table 1, it can be seen that Zr represents only about 10% of the total composition of the topmost layers.

Fig. 4a shows a shift in the Ag3d for the ZrNO–Ag co-sputtered (90 s) sample from a binding energy (BE) 364.7–365.4 eV within the 45 min *E. coli* inactivation period. This reflects $Ag^{1+}/Ag^{2+}$ redox reactions taking place on the sample surface during the bacterial inactivation [41]. Fig. 4b shows the Zr-peak of the ZrNO–Ag (90 s) sample shifting from a BE 181.6 eV to a BE 182.7 eV within the 45 min bacterial inactivation time, involving $Zr^{4+}/Zr^{3+}$ redox reactions when the sample interacts with bacteria [42].

### 3.7. Sample reusability and ions release during bacterial inactivation detected by ICPS

Fig. 5 shows the reuse of the co-sputtered ZrNO–Ag (90 s) sample during *E. coli* bacterial inactivation. Fig. 5 shows that after 8 cycles, the samples kept their initial performance. After the first and second recycling the discontinuity in the abscissa shows the non-sequential kinetics for the 4th and 8th recycling conserving the initial loss of viability kinetics. The inactivation bacterial time remained within 40–45 min.

The surface atomic percentage concentration of elements in the ZrNO–Ag (90 s) sputtered samples after being contacted 3 s with bacteria were: O1s 8.8%; N1s 2.3%; C1s 54.9%; Zr3d 2.8% and Ag3d 35.4%. These percentages did vary less than 10% during the 40 min reaction leading to the total bacterial loss of viability. Therefore, the rapid destruction of the fragments of bacterial decomposition during the photocatalysis accounts for the constant rate observed for the total loss of viability reported in Fig. 5.

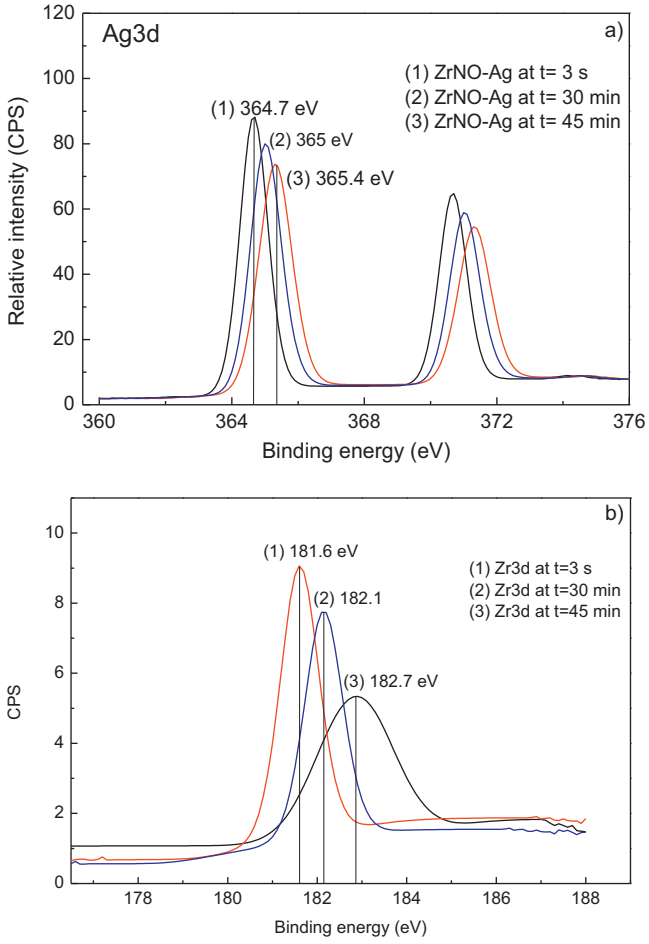


**Fig. 4.** (a) XPS shift of the Ag-doublets for the co-sputtered ZrNO–Ag (90 s) sample within the 45 min period of bacterial inactivation. (b) Zr peak-shift during *E. coli* inactivation for the co-sputtered ZrNO–Ag (90 s) sample within the 45 min bacterial inactivation.

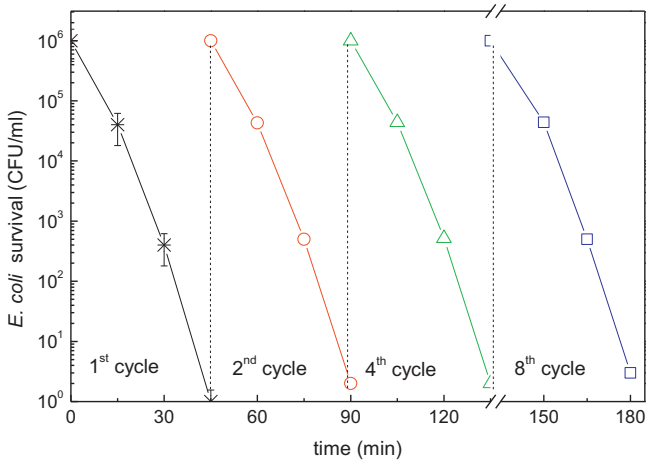


**Fig. 5.** Cycling of a ZrNO–Ag (90 s) samples leading to the total loss of bacterial viability under Osram Lumilux 18 W/827 (400–700 nm) irradiation.

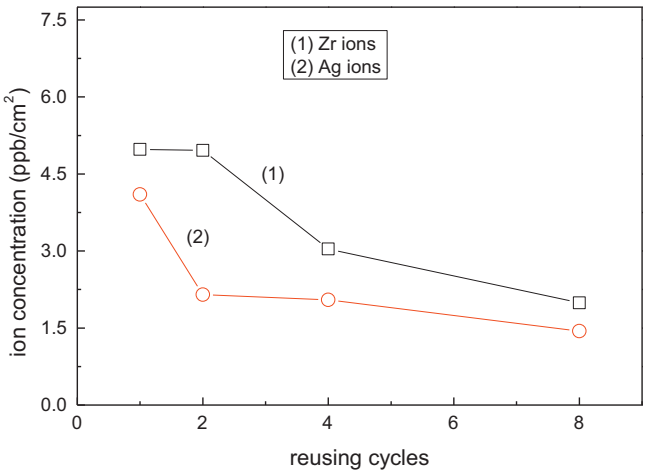


**Fig. 6.** Ion-coupled plasma mass spectrometry (ICP-MS) determination of Ag-ions and Zr-ions released from a co-sputtered ZrNO–Ag (90 s) within the *E. coli* loss of bacterial viability.

Fig. 6 shows the Ag- and Zr-ions concentrations released during the reuse of ZrNO–Ag (90 s) sputtered samples. The Ag-ions release during 8 cycles was <5 ppb/cm$^2$, which is below the allowed cytotoxicity levels of 35–90 ppb/cm$^2$ [43]. Therefore, the bacterial inactivation mediated by ZrNO–Ag (90 s) does not introduce cytotoxicity but proceeds through an oligodynamic effect.

### 3.8. Electron microscopy (TEM) and EDX of ZrNO–Ag (90 s) co-sputtered sample

Fig. 7a presents the TEM of a co-sputtered ZrNO–Ag (90 s) sample on polyester. In the left-hand side the Zr and Ag are shown to be immiscible when co-sputtered on the polyester fibers. The right-hand side Fig. 7a shows the Zr and Ag-nanoparticles contrasted by high angular annular dark field (HAADF). The sizes of the $ZrO_2$ and Ag nanoparticles in the co-sputtered ZrNO–Ag (90 s) sample were respectively 80–130 nm and 8–15 nm. Fig. 7b presents the different microstructure to the one seen for the co-sputtered samples. Two well-defined bands of sequentially sputtered ZrNO (90 s) and Ag (20 s) were observed.

Due to its size, the Ag nanoparticles are not able to penetrate to bacteria core through the bacterial porins with diameters of 1–1.3 nm [44,45]. Only Ag-ions diffuse through bacterial porins leading to DNA damage and finally to bacterial inactivation [9].

### 3.9. Suggested reaction mechanism

The $ZrO_2$ species has been deconvoluted as described in the XPS section for the ZrNO–Ag (90 s) sample. All metals with exception of Hg are known to form surface hydroxide in contact with

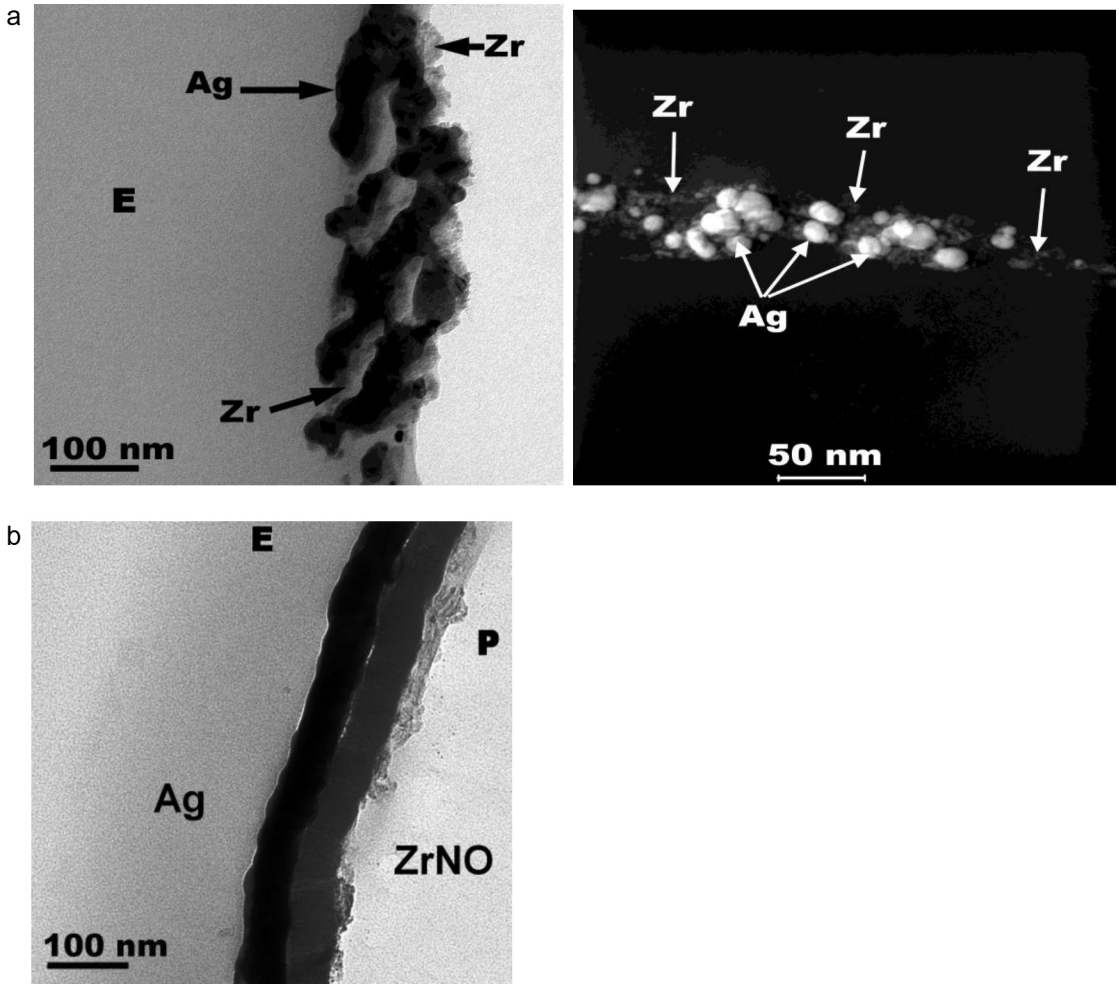


**Fig. 7.** (a) Left-hand side: transmission electron microscopy of a co-sputtered ZrON–Ag (90 s) sample (amplification 28k). Right side: the same sample in high angular annular dark field (HAADF) representation. (b) EM of sequential sputtering of ZrNO (90 s) followed by sputtering of Ag (20 s).

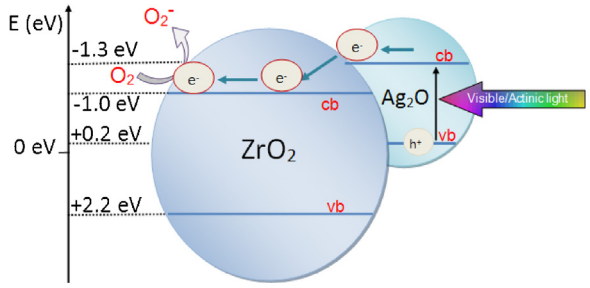


**Fig. 8.** Scheme of the electron injection from $Ag_2O$ to $ZrO_2$ under visible light.

air containing water vapor. ZrNO–Ag samples forms AgOH on its surface. The favorable decomposition of AgOH leads to $Ag_2O$ as in (Eq. (1)) [46].

$$AgOH \rightarrow Ag_2O + H_2O(pk = 2.87) \quad (1)$$

$Ag_2O$ is thermodynamically stable at pH 6–7 where the bacterial inactivation of *E. coli* is shown to proceed in Fig. 1a–c. For mechanistic considerations of the $ZrO_2/Ag_2O$ under visible light we consider next the energy level of $Ag_2O$ and $ZrO_2$. The $ZrO_2$ nanoparticles in Fig. 7 present sizes of ~100 nm and these nanoparticles have been reported with a band-gap (bg) ~3.2 eV [35], a conduction band (cb) at −1.0 eV NHE and a valence band (vb) at +2.2 eV NHE [36]. Visible light photo-activates the semiconductor $Ag_2O$ with $1.46 < bg < 2.25$ eV [47,48]

$$Ag_2O + light \rightarrow Ag_2O(h_{vb}^{+}) + Ag_2O(e_{cb}^{-}) \quad (2)$$

The bacterial inactivation kinetics reported in Fig. 1c suggests that the interfacial charge transfer process (IFCT) [49] in the co-sputtered ZrNO–Ag film proceeds more readily compared to the sequential sputtered ZrNO–Ag sample (Fig. 1b) due to the shorter distance between Zr and Ag inducing higher quantum efficiency. Donor–acceptor pair interactions depend on the charge diffusion distance and this is a function of the particle size and shape in the film microstructure.

Under visible light, the transfer of charge from $Ag_2O$ to $ZrO_2$ is thermodynamically favorable. The $Ag_2O_{cb}$ is −1.3 eV NHE at pH 0. The vb of $Ag_2O$ +0.2 eV NHE at pH 0 [47–49] lie above the $ZrO_2$ presenting a conduction band (cb) at −1.0 eV and the valence band (vb) at +2.2 eV. The electrons in the $Ag_2O_{cb}$ inject electron into the $ZrO_{2cb}$ since they are situated at a higher energetic level. The electrons in Eq. (2) react with $Ag_2O$

$$2Ag_2O + e^{-} \rightarrow 4Ag^{0} + O_2^{-} \quad (3)$$

We suggest that $O_2$ Eq. (3) promote the reactions (5) and (6) producing highly oxidative radicals, while the $h^+$ in Eq. (2) would react with $H_2O$ (water vapor) as shown below in Eq. (4). This reaction runs parallel with Eq. (5) generating OH° radicals or other highly reactive oxidative radicals able to inactivate *E. coli*. The $h_{vb}^{+}$ in Eq. (4) originate from the $Ag_2O$ nanoparticles in Eq. (2)

$$h_{vb}^{+} + H_2O \rightarrow OH^{\circ} + H^{+} \quad (4)$$

$$e_{cb}^{-} + H_2O + O_2 \rightarrow OH^{\circ} + OH^{-} + 1/2O_2^{-} \quad (5)$$

$$e_{cb}^{-} + O_2 \rightarrow O_2^{\bullet -} \quad (6)$$

We show in Fig. 8 a scheme for the charge transfer discussed in the preceding paragraphs to better visualize the photo-induced electron injection from $Ag_2O$ into $ZrO_2$ induced under visible light.

## 4. Conclusions

Zr-oxynitride films on polyester have been deposited by sputtering methods. This study presents the effect of visible light induced processes on *E. coli* inactivation. The ZrNO–Ag XPS envelope was deconvoluted showing $ZrO_2$, ZrNO, and ZrN. The most suitable bacterial inactivation under light was attained with the ZrNO–Ag co-sputtered samples on polyester for 90 s. Bacterial inactivation kinetics of *E. coli* depends on the amount of Ag on the polyester and if sequential or simultaneous sputtering of ZrNO and Ag was applied. The fasts co-sputtering of ZrNO and Ag presented a thickness below the addition of the individual ZrNO and Ag-layers obtained by sequential sputtering of ZrNO and Ag. The repetitive bacterial inactivation the ZrNO–Ag polyester samples provided evidence for the stability and adhesion of the samples. The optical absorption of the ZrNO and ZrNO–Ag samples was found to be directly proportional to the *E. coli* inactivation kinetics under low intensity actinic light. A possible reaction mechanism is suggested based on the energetic band levels of $Ag_2O$ and $ZrO_2$. The ZrNO-sputtered polyester showed also a significant bactericide effect. This is important since these later surfaces avoid the leaching of the heavy Ag-metal into the environmental, a matter of growing environmental concern.

## Acknowledgments

We thank the COST Action MP0804 Highly Ionized Impulse Plasma Processes (HIPIMS), the EPFL and LIMPID 7 FP Collaborative European Project Nanocomposite Materials for Photocatalytic Degradation of Pollutants NMP 2012.2.2.2-6 (n. 310177) for financial support of this work.

## References

[1] Thüringer Surface and Biomaterials Kolloquium, 13–15 September 2011, Zeulenroda, Germany.
[2] J. Bourn, Improving patient care by reducing the risk of hospital acquired infection: A progress report, National Audit Office, 2003-2004.
[3] R. Plowman, R. Graves, N. Griffin, L. Taylor, Journal of Hospital Infection 47 (2001) 198–204.
[4] S. Dancer, Journal of Hospital Infection 73 (2009) 378–386.
[5] A. Kramer, I. Schwebke, G. Kampf, Diseases 6 (2006) 137–146.
[6] A. Mills, C. Hill, P. Robertson, Journal of Photochemistry and Photobiology A 237 (2012) 7–23.
[7] K. Page, M. Wilson, P.I. Parkin, Journal of Materials Chemistry 19 (2009) 3819–3831.
[8] S. Noimark, Ch Dunnill, M. Wilson, P.I. Parkin, Chemical Society Reviews 38 (2009) 3435–3448.
[9] C. Page, M. Wilson, N. Mordan, W. Chrzanowski, J. Knowles, P.I. Parkin, Journal of Materials Science 46 (2011) 6355–6363.
[10] K. Page, R. Palgrave, P.I. Parkin, M. Wilson, Sh. Savin, Journal of Materials Chemistry 17 (2007) 95–104.
[11] H.A. Foster, P. Sheel, W.D. Sheel, P. Evans, S. Varghese, N. Rutschke, M.H. Yates, Journal of Photochemistry and Photobiology A 216 (2010) 283–289.
[12] M.S.P. Dunlop, P.C. Sheeran, A.J.M. Byrne, S.A. McMahon, M.A. Boyle, G.K. McGuigan, Journal of Photochemistry and Photobiology A 216 (2010) 303–3010.
[13] M.H. Yates, A.L. Brook, B.I. Ditta, P. Evans, H.A. Foster, D.W. Sheel, A. Steele, Journal of Photochemistry and Photobiology A 197 (2008) 197–2008.
[14] P. Kelly, H. Li, P. Benson, K. Whitehead, J. Verran, R. Arnell, I. Iordanova, Surface & Coatings Technology 205 (2010) 1606–1610.
[15] P. Kelly, H. Li, K. Whitehead, J. Verran, R. Arnell, I. Iordanova, Surface & Coatings Technology 204 (2009) 1137–1141.
[16] L. Zhang, R. Dillert, D. Bahnemann, Energy & Environmental Science 5 (2012) 7491–7507.
[17] A. Fujishima, T. Rao, D. Tryk, Journal of Photochemistry and Photobiology C: Reviews 1 (2009) 1–21.
[18] W. Tung, W. Daoud, Journal of Materials Chemistry 21 (2011) 7858–7869.
[19] P.V. Kamat, Accounts of Chemical Research 45 (2012) 1906–1915.
[20] J. Kiwi, V. Nadtochenko, Journal of Physical Chemistry B 108 (2004) 17675–17684.
[21] V. Nadtochenko, A. Rincon, S. Stanka, J. Kiwi, Journal of Photochemistry and Photobiology A 169 (2009) 131–137.
[22] R. Bacsa, J. Kiwi, T. Ohno, P. Albers, V. Nadtochenko, Journal of Physical Chemistry B 109 (2005) 5994–6003.
[23] J. Kiwi, V. Nadtochenko, Langmuir 21 (2005) 4631–4641.
[24] H. Foster, I. Ditta, S. Varghese, A. Steele, Applied Microbiology and Biotechnology 90 (20) (2013) 1847–1868.
[25] O.K. Dalrymple, E. Stefanakos, M. Trotz, D. Goswami, Applied Catalysis B: Environmental 98 (2010) 27–38.

[26] S. Pigeot-Rémy, F. Simonet, E. Errazuriz-Cerda, J. Lazzaroni, D. Atlan, C. Guillard, Applied Catalysis B: Environmental 104 (2011) 390–398.
[27] A. Markowska-Szczupak, K. Ulfig, A. Morawski, Catalysis Today 169 (2011) 249–257.
[28] L. Rio, E. Kusiak, J. Kiwi, C. Pulgarin, A. Trampuz, A. Bizzini, Journal of Applied Microbiology 78 (2012) 8176–8182.
[29] K. Sarakinos, J. Alami, D. Konstantinidis, Surface & Coatings Technology 204 (2010) 1661–1684.
[30] E. Nieh, C. Kang, H. Cho, K. Onishi, R. Choi, S. Krishnan, J. Han, Y. Kim, J. Akbar, C. Lee, IEEE Transactions on Electron Devices 50 (2003) 333–340.
[31] B. Brandt, D. Liu, L. Rubin, Review of Scientific Instruments 70 (1999) 104–110.
[32] E. Ariza, L.A. Rocha, F. Vaz, L. Cunha, S.C. Ferreira, P. Carvalho, L. Rebouta, E. Alves, Ph. Goudeau, J.P. Riviere, Thin Solid Films 469–470 (2004) 274–281.
[33] P. Carvalho, F. Vaz, L. Rebouta, L. Cunha, C.J. Tavares, C. Moura, E. Alves, A. Cavaleiro, Ph Goudeau, E. Le Bourhis, J.P. Rivière, J.F. Pierson, O. Banakh, Journal of Applied Physics 98 (2005) 023715.
[34] F. Vaz, P. Carvalho, L. Cunha, L. Rebouta, C. Moura, E. Alves, A.R. Ramos, A. Cavaleiro, Ph. Goudeau, J.P. Rivière, Thin Solid Films 469–470 (2004) 11–17.
[35] A. Emeline, G. Kateva, V. Rudakova, N. Ryabchuk, N. Serpone, Langmuir 14 (1998) 5011–5022.
[36] K. Sayama, H. Arakawa, Journal of Physical Chemistry 97 (1993) 531–533.
[37] S. Rtimi, O. Baghriche, R. Sanjines, C. Pulgarin, M. Ben-Simon, J.-C. Lavanchy, A. Houas, J. Kiwi, Applied Catalysis B: Environmental 123–124 (2012) 306–315.
[38] C. Gunawan, W. Teoh, C. Marquis, J. Lifia, R. Amal, Small 5 (2009) 341–347.
[39] H. Wiame, M. Centeno, M. Picard, S. Bastians, P. Grange, Journal of the European Ceramic Society 18 (1998) 1293–1927.
[40] A. Rizzo, M. Signore, L. Mirenghi, T. Di Luccio, Thin Solid Films 517 (2009) 5956–5964.
[41] M.-I. Mejía, G. Restrepo, M. Marín, R. Sanjinés, C. Pulgarín, J. Mielczarski, E. Mielczarski, J. Kiwi, ACS Applied Materials & Interfaces 2 (2010) 230–235.
[42] D.C. Wagner, M.W. Riggs, L.E. Davis, G.E. Müllenberg (Eds.), Handbook of X-ray Photoelectron Spectroscopy, Perkin-Elmer Corp. Phys. Electr. Div., Minnesota, 1979.
[43] A. Ewald, S.K. Glückerman, R. Thull, U. Gbureck, Biomedical Engineering (Online) 5 (2006) 20–32.
[44] H. Nikaido, The Journal of Biological Chemistry 269 (1994) 3905–3908.
[45] P. Asharani, G. Mun, M. Hande, V. Valiyavettil, ACS Nano 3 (2009) 279–290.
[46] M. Pourbaix, Atlas of Electrochemical Equilibria in Aqueous Solutions, NACE Int Texas, USA, 1976.
[47] Y. Ida, T. Watase, M. Shinagawa, M. Watabanbe, M. Chigane, M. Inaba, A. Tasaka, M. Izaki, Chemistry of Materials 20 (2008) 1254–1256.
[48] A. Varkey, Solar Energy Materials and Solar Cells 29 (1993) 253–259.
[49] H. Irie, S. Miura, K. Kamiya, K. Hashimoto, Chemical Physics Letters 457 (2008) 202–207.